# Bright and stable near infra-red fluorescent protein for *in vivo* imaging

**Grigory S. Filonov**[1], **Kiryl D. Piatkevich**[1], **Li-Min Ting**[2], **Jinghang Zhang**[3], **Kami Kim**[2], and **Vladislav V. Verkhusha**[1]

[1]Department of Anatomy and Structural Biology and Gruss-Lipper Biophotonics Center, Albert Einstein College of Medicine, Bronx, New York 10461

[2]Department of Medicine and Department of Microbiology and Immunology, Albert Einstein College of Medicine, Bronx, New York 10461

[3]Flow Cytometry, Core Facility, Albert Einstein College of Medicine, Bronx, New York 10461

## Abstract

The ability of non-invasive monitoring of deep-tissue developmental, metabolic, and pathogenic processes will advance modern biotechnology. Imaging of live mammals using fluorescent probes is more feasible within a "near-infrared optical window" (NIRW)[1]. Here we report a phytochrome-based near infra-red fluorescent protein (iRFP) with the excitation/emission maxima at 690/713 nm. Bright fluorescence in a living mouse proved iRFP to be a superior probe for non-invasive imaging of internal mammalian tissues. Its high intracellular stability, low cytotoxicity, and lack of the requirement to add external biliverdin-chromophore makes iRFP as easy to use as conventional GFP-like proteins. Compared to earlier phytochrome-derived fluorescent probes, the iRFP protein has better *in vitro* characteristics and performs well in cells and *in vivo*, having greater effective brightness and photostability. Compared to the far-red GFP-like proteins, iRFP has substantially higher signal to background ratio in a mouse model owing to its infra-red shifted spectra.

Imaging in mammals using fluorescent proteins (FPs) is an important technique to quantitatively and non-invasively track tumor growth and metastasis, gene expression, angiogenesis, and bacterial infection[2]. Deep tissues visualization of the conventional FPs derived from the Green Fluorescent Protein family (GFP-like FPs) is still hindered by the high absorbance of hemoglobin and skin melanin. An optimal FP for *in vivo* imaging should have both excitation and emission maxima within a NIRW from approximately 650 nm to

900 nm, which has the lowest tissue absorbance[1]. However, to this moment even the most far-red shifted GFP-like proteins still have excitation spectra outside of the NIRW.

To circumvent these problems, near infra-red (NIR) FPs can be engineered on the basis of phytochromes[3]. Phytochromes are photosensory receptors absorbing light in the red and far-red part of spectrum[4]. The family of phytochromes shares a conserved photosensory protein core consisting of a PAS domain, a GAF domain, and a PHY domain. A linear tetrapyrrole chromophore, such as biliverdin IXα (BV), phycocyanobilin or phytochromobilin, is covalently bound to one of the first two domains. Bacteriophytochromes are more advantageous for use as design templates for NIR FPs since BV, an obligatory co-factor of bacteriophytochromes, is a component of normal mammalian heme metabolism[5].

Fluorescent properties of phytochromes have been known for a long time[3,6-8] but only recently a NIR fluorescent mutant of the *Dr*BphP bacteriophytochrome from *Deinococcus radiodurans* named IFP1.4 was reported to be useful for *in vivo* liver visualization[9]. However the properties of IFP1.4 remain suboptimal and require development of new superior probes.

In order to engineer NIR FP we turned to another template – bacteriophytochrome *Rp*BphP2[10] from the photosynthetic bacterium *Rhodopseudomonas palustris*. The full-length *Rp*BphP2 protein is weakly fluorescent at 725 nm when excited at 710 nm[10].

First, we truncated *Rp*BphP2 to retain the PAS and GAF domains (*Rp*BphP2-PAS-GAF; 316 amino acids in length) and introduced D202H mutation, since substitutions of this aspartic acid had been shown to improve fluorescent properties of the phytochromes[8,11]. Expression of this *Rp*BphP2-PAS-GAF/D202H variant in bacteria co-transformed with a plasmid bearing a heme-oxygenase gene (to produce BV co-factor) proved its initial fluorescence.

Then *Rp*BphP2-PAS-GAF/D202H variant was subjected to three rounds of random mutagenesis followed by a round of saturating mutagenesis of the identified key residues. The final mutant had the following 13 substitutions: S13L, A92T, V104I, V114I, E161K, Y193K, F198Y, D202T, I203V, Y258F, A283V, K288T, and N290Y (Supplementary Fig. 1). This variant was named an iRFP (infra-Red Fluorescent Protein).

Compared to IFP1.4, iRFP exhibited a higher extinction coefficient (Fig. 1a and Table 1) as determined by direct measurement of the protein concentrations, while extinction coefficients calculated based on the comparison[9] of absorbance of the proteins and free BV at 391 nm were similar. iRFP fluorescence exhibited the excitation/emission maxima at 690/713 nm (Fig. 1b), slightly red-shifted compared to IFP1.4. Quantum yields at pH 7.5 were measured to be 5.9% for iRFP and 7.7% for IFP1.4. Based on these measurements the relative molecular brightness of iRFP is 1.2 of that of IFP1.4 (Table 1).

iRFP had slightly slower maturation at 37°C than IFP1.4 with a maturation half-time of 2.8 hours versus 1.9 hours for IFP1.4 (Fig. 1c and Table 1). The fluorescence of iRFP was pH stable with $pK_a$ value of 4.0, compared to $pK_a$ of 4.6 for IFP1.4 (Fig. 1d and Table 1).

Size-exclusion chromatography demonstrated that iRFP was a dimer while IFP1.4 contained two fractions: the monomeric and oligomeric with an apparent MW of ~190 kDa (Supplementary Fig. 2). Revealed IFP1.4 oligomers may also exist in mammalian cells potentially limiting IFP1.4 use as a fusion tag. In contrast, iRFP exhibited a clear dominant dimer peak and subsequent tandem engineering strategy[12] may enable iRFP to be useful as a fusion tag.

Quasi-equilibrium curves of guanidinium chloride (GndCl) induced protein unfolding[13] demonstrated that iRFP had higher, compared to IFP1.4, conformation stability (Table 1 and Supplementary Fig. 3a). The calculated difference in free energies of unfolding[14,15] between the iRFP and IFP1.4 proteins was 3.5 kcal/mole. Since iRFP and IFP1.4, as other phytochromes[5], bind BV covalently (Supplementary Fig. 4), GndCl-induced fluorescence decrease indicates the loss of proteins' tertiary structures rather than BV dissociation indicating that iRFP is substantially more thermodynamically stable.

The normalized photostability of iRFP, measured in aqueous drops in oil, was substantially higher than that for IFP1.4, with the difference being ~10-fold (Supplementary Fig. 3b and Table 1). To exclude the possibility that both proteins revealed phytochromes photoswitching properties instead of bleaching, the aqueous drops irradiated with photobleaching light were left in the dark for additional 30 minutes and were then imaged again (Supplementary Fig. 3b). Neither protein showed any increase in fluorescence suggesting that both remained in the main, non-photoswitched state and that the observed loss of fluorescence was caused by photobleaching.

Two-photon (2P) excitation spectrum of purified iRFP measured in 1100-1340 nm spectral region revealed excitation peak at 1260 nm corresponding to the main one-photon absorbance maximum (Supplementary Fig. 5). Thus iRFP is also suitable for the multiphoton imaging though its 2p properties remain to be studied further.

To characterize iRFP in mammalian cells, we FACS analyzed HeLa cells transiently transfected with iRFP and IFP1.4 encoding plasmids (no exogenous heme-oxygenase gene was used here). Cells were also co-transfected with EGFP plasmid for subsequent NIR signal normalization. Since amount of endogenous BV might not be enough to bind to all produced NIR proteins, where indicated the saturating concentration[9] of 25 μM of BV was added to culture medium 2 hours before analysis.

Despite slight differences in molecular brightness of the phytochromes, the fluorescence signals of the iRFP and IFP1.4 expressing cells differed drastically (Fig. 1e,f). While the iRFP cells showed bright fluorescence even without addition of exogenous BV, the IFP1.4 fluorescence was observed only in the cells expressing EGFP at high levels and in the presence of exogenous BV. Quantification of this difference, performed by normalizing phytochrome signal to EGFP signal, showed that iRFP cells were 13-fold brighter than the IFP1.4 cells without exogenous BV and 7-fold brighter after addition of BV (Fig. 1g and Supplemetary Table 1). Therefore the effective brightness of iRFP in living cells, which is a combination of molecular brightness, intracellular stability, affinity for BV, and protein expression level, is substantially higher than that of IFP1.4. To compare relative

concentrations of the produced fluorescent molecules of iRFP and IFP1.4, the normalized cellular fluorescence intensities were divided by the respective molecular brightness. The cellular amount of the iRFP fluorescent molecules was 5.9-fold and 11.0-fold greater than that of IFP1.4 with and without exogenous BV, respectively (Supplemetary Table 1).

Epifluorescent microscopy of the transiently transfected HeLa cells showed evenly dispersed fluorescent signals without any intracellular aggregates for both proteins (Fig. 1h). Addition of exogenous BV and 4-fold longer exposure times were typically required to obtain images of the IFP1.4 cells of the same brightness as images of the iRFP cells without exogenous BV. The normalized intracellular photostability of iRFP was even higher than in aqueous drops while the photostability of IFP1.4 was similar, with an overall difference between two proteins ~30-fold (Fig. 1i and Supplemetary Table 1).

In order to assess the degradation kinetics of iRFP and IFP1.4 cells expressing one or another protein were treated with 1 mM of a puromycin to inhibit protein translation[16]. The fluorescence of both proteins was stable in cells and exhibited similar degradation time-courses over a period of 20 hours (Fig. 1j).

Since the brightness of the IFP1.4 cells increased more upon BV addition than that of the iRFP cells (Fig. 1g), we studied whether the proteins had different BV binding efficiencies. Different BV concentrations were added to the HeLa cells expressing either IFP1.4 or iRFP and the BV-binding curves (Fig. 1k) were fitted and processed using a Scatchard equation[17]. The BV dissociation constants for iRFP and IFP1.4 were 0.35 μM and 4.2 μM, respectively (Supplementary table 1). The data suggest that the 12-fold higher iRFP binding affinity allows efficient formation of iRFP-BV fluorescent complexes utilizing relatively low concentrations of endogenous BV produced in cells.

To assess intracellular stability of the iRFP and IFP1.4 apoproteins, we expressed iRFP and IFP1.4 in HeLa cells without or with exogenous BV added for a short (2 hours) or long (42 hours) periods of time before the essay. Expression of IFP1.4 in presence of BV during 42 hours resulted in cells that were twice as fluorescent compared to cells maintained with BV just for 2 hours. In contrast, prolonged BV exposure had no effect on the amount of iRFP fluorescence (Fig. 1l and Supplementary table 1). Similar results were obtained by expressing the proteins in bacteria bearing the heme-oxygenase without and with added heme precursors (Supplementary Fig. 6). Overall, these data suggested that BV binding to IFP1.4 apoprotein was required to stabilize it, possibly by preventing from intracellular degradation. At the same time the majority of the iRFP apoprotein molecules remained intact during 2 days as suggested by the same brightness of the iRFP cells exposed to exogenous BV for short and long time periods (Fig. 1l).

To study toxicity of both proteins in mammalian cells an approach used for GFP-like proteins was applied[18]. iRFP, IFP1.4 and control GFP/S65T variant were transiently expressed for 1, 3, and 5 days, and the mean fluorescence intensity of the viable cells at each day was determined using FACS (Supplementary Fig. 7). If the FPs were cytotoxic then the fluorescent intensity of the expressing cells would rapidly decrease[18]. In agreement with the previous data[19,20] the GFP-producing cells demonstrated a "bell-shaped" profile of the

expression. In contrast, the apparent expression of iRFP and IFP1.4 steadily increased during 5 days. We attributed this increase to a combination of two processes: the high-level production of exogenous apoproteins and a 'catching up' synthesis of endogenous BV to bind it, thus, forming the fluorescent holoproteins.

These results prompted us to look for longer expression conditions where the holoprotein level could remain constant. For this purpose preclonal mixtures of HeLa cells expressing iRFP, E2-Crimson (non-cytotoxic standard)[21] or mKate2 (cytotoxic standard)[21] were made. Prolonged expression of IFP1.4 at detectable levels required constant BV addition that might affect the results; therefore, it was not assessed in this assay. Cells with iRFP, E2-Crimson, or mKate2 were maintained for 21 days after the transfection with a selection drug, then sorted, and finally analyzed after 20 more days being under the selection. E2-Crimson and iRFP sorted cell populations remained mostly within the original sorting gates while the majority of the sorted mKate2 cells lost their fluorescence (Supplementary Fig. 8). Since iRFP expressing cells behaved similarly to the cells expressing non-cytotoxic control E2-Crimson we concluded that iRFP was not cytotoxic.

Next iRFP applicability for imaging in mammals was tested. Mice were infected with adenoviral particles containing either iRFP or IFP1.4 genes and then imaged using IVIS Spectrum imager. Fluorescence of the liver in the iRFP infected mice was detected starting the second day post-infection, with the peak intensity at day 5 (Fig. 2a). The IFP1.4 expressing mice showed weak liver fluorescence during all days of imaging. At day 5 post-infection both mice were administrated 250 nmol of BV. After the injection, the IFP1.4 infected liver become ~4-fold brighter; however, it still was dimmer than the iRFP expressing liver. Calculation of total radiant efficiencies of the liver regions demonstrated the iRFP effective brightness *in vivo* being 22-fold higher without exogenous BV and 7-fold higher after the BV injection (Fig. 2b).

Following BV administration, the IFP1.4 liver fluorescence lost half of its brightness after ~30 hours and returned to the initial brightness ~2 days after the injection (Fig. 2c). The decrease in brightness of the iRFP liver during the 2 day period after the BV injection was ~10% only. These data suggest that in contrast to iRFP, prolonged mouse experiments involving IFP1.4 will require frequent BV injections.

Correct localization of both proteins was revealed by *ex vivo* imaging of the isolated livers (Fig. 2d). Importantly, the iRFP fluorescence was easily detected in the liver 10 days post-infection without administrating BV during this period (Fig. 2e), suggesting that iRFP is both stable and non-cytotoxic *in vivo*.

iRFP expression in other than liver tissues with no need for exogenous BV was demonstrated by *ex vivo* imaging of the spleen excised from the infected mouse (Supplementary Fig. 9).

In order to additionally support general applicability of iRFP for different body tissues expression, the liver cells isolated from iRFP-infected and control mice were subjected to FACS analysis. Then iRFP fluorescence level of these primary hepatocytes was compared to that of the stably iRFP-expressing *in vitro* cultured cells originated from human cervix, rat

brain, and rat mammary gland. The cultured cells stably expressed iRFP with the similar, compared to liver, or even higher fluorescence brightness without adding exogenous BV (Supplementary Fig. 10) suggesting that iRFP is suitable for imaging of various organs and tissues, owing to its high affinity to endogenous BV.

Molecular evolution approach enabled us to develop an advanced NIR FP with excitation and emission maxima inside of the NIR window. This genetically-encoded iRFP probe should dramatically improve *in vivo* studies of small mammals.

iRFP has superior properties compared to the IFP1.4 protein. Firstly, iRFP has higher molecular brightness and greater photostability. Secondly, iRFP exhibits greater thermodynamic stability, lower $pK_a$ value, and higher binding affinity to BV. Thirdly, iRFP has significantly higher effective brightness in cells and in mice since IFP1.4 apoprotein has lower affinity to BV and is not stable without it. Lastly, iRFP does not require addition of an external BV when imaged in mammalian cells, and in this respect, it behaves similarly to GFP-like proteins.

Several GFP-like far-red FPs have been shown to be useful for the whole-body imaging[22,23] however their spectral properties are suboptimal for this purpose. To directly compare iRFP deep-tissue imaging performance with that of far-red shifted FPs, such as mKate2[24], E2-Crimson[21], mNeptune[22], TagRFP657[25], and eqFP670[23], we imaged the same amount of purified proteins at 7.0 and 18.1 mm depth inside of a mouse phantom, which has the autofluorescence and light-scattering properties matching those of a mouse muscle tissue[26,27] (Fig. 3a,c). To compare brightness in different spectral channels, a signal-to-background ratio for the FPs for each channel was calculated. The highest ratio values among the different channels are shown (Fig. 3b,d). iRFP has 2.4-fold and 3.2-fold larger ratio values at 7.0 mm and 18.1 mm depth, respectively, than the second in a row mNeptune. The data confirmed that the far-red shifted spectra allow iRFP to perform substantially better despite being less bright on the molecular level.

In conclusion, currently iRFP is, both in terms of molecular and effective brightness, the brightest phytochrome-based and the most infra-red shifted FP. iRFP is stable, non-cytotoxic and utilizes the low concentrations of endogenous BV to be visualized in cells, tissues, and mammals. These features make its application as easy as the conventional GFP-like FPs, and hence should significantly broaden the possibilities of non-invasive *in vivo* imaging.

## Supplementary Material

Refer to Web version on PubMed Central for supplementary material.

## ACKNOWLEDGEMENTS

## METHODS

### Mutagenesis and screening of libraries

A *Rp*BphP2 gene[10] was kindly provided by Eric Giraud (Institute for Research and Development, France). IFP1.4 gene was *de novo* synthesized by GenScript Company, based on the available protein sequence[9]. The DNA sequence was optimized with proprietary OptimumGene™ algorithm (GenSript), taking into account the codon usage bias (human cells), GC content, CpG dinucleotides content, mRNA secondary structure, and other parameters.

The genes encoding a bacteriophytochrome *Rp*BphP2 and an IFP1.4 protein were amplified using polymerase chain reaction (PCR) as the *Bgl*II-*Eco*RI or *Pst*I-*Hind*III fragments and inserted into the *Bgl*II-*Eco*RI sites of a pBAD/His-B vector or the *Pst*I and *Hind*III sites of a pBAD/His-C vector, respectively (Invitrogen). Biliverdin synthesis in bacteria was facilitated by co-transformation with a pPL-BV plasmid, which was obtained after digestion with *Bam*HI and subsequent ligation of the pPL-PCB plasmid[28]. The pPL-PCB plasmid was kindly provided by Drs. Andrew Ulijasz and Richard Vierstra (University of Wisconsin, USA).

Site specific mutagenesis was performed using a QuickChange Mutagensis Kit (Stratagene). For simultaneous mutagenesis at several positions, including a site-specific saturated mutagenesis (i.e., all 20 amino acids were encoded using the mixture of primers), an overlap-extension method was applied[29]. Random mutagenesis was performed with a GeneMorph II Random Mutagenesis Kit (Stratagene), using conditions that resulted in the mutation frequency of up to 16 mutations per 1,000 base pairs. After the mutagenesis, a mixture of mutants was electroporated into the LMG194 host cells (Invitrogen) containing the pPL-BV plasmid.

Typical mutant libraries for FACS screens consisted of $10^7$-$10^8$ independent clones.

LMG194 bacteria were grown overnight in LB medium with an addition of 2% glucose to repress synthesis of both proteins. Next morning, the bacterial cells were centrifuged and re-suspended in RM medium with 0.002% arabinose, 0.001 mM IPTG, 100 μM 5-aminolevulinic acid (ALA), and 50 μM $FeCl_3$. The cells were then grown up to 24 hours either at 37°C or 37°C followed by 25°C, depending on the experiment.

For FACS screening, protein mutants were expressed in bacteria at 37°C followed by an overnight incubation at 25°C. The next morning, bacteria were washed with Phosphate Buffered Saline (PBS) and then diluted with PBS to an optical density of 0.02 at 600 nm. A MoFlo XDP cell sorter (Beckman Coulter), equipped with the standard Ar, Kr, Ar-Kr mixed-gas lasers (Coherent) and a 592 nm solid-state laser (MPB Communications), was used. Typically, about 10 sizes of each library were FACS-sorted, using a 676 nm Kr laser line for excitation and a 700LP nm emission filter for positive selection. The brightest

collected NIR bacterial cells were rescued in a SOC medium at 37°C for one hour, and then plated on Petri dishes made of RM/agar supplemented with ampicillin and kanamycin. The next day, the expression of proteins in bacterial colonies on the dishes were induced with 0.002% of arabinose and 0.001mM of IPTG. The dishes were left for 4-6 hours at 37°C and then incubated at room temperature overnight.

Fluorescence of the colonies was analyzed the next day using a Leica MZ16F fluorescence stereomicroscope equipped with the 650/45 nm excitation and 690LP nm emission filters (Chroma), and a CCD camera. The 20-30 brightest clones were selected and their DNA was sequenced. A mixture of several selected mutants was then utilized as a template for the next round of mutagenesis.

## Protein characterization *in vitro*

*Rp*BphP2 mutants and IFP1.4 protein with polyhistidine tags were expressed in LMG194 bacterial cells, as described above, and then purified using Ni-NTA agarose (Qiagen). The excitation and emission spectra were measured using a FluoroMax-3 spectrofluorometer (Jobin Yvon). For absorbance measurements, a Hitachi U-2000 spectrophotometer was used.

Two different approaches were utilized to determine extinction coefficients. The first approach was based on a direct measurement of the protein concentrations with a BCA Protein essay kit (Pierce), followed by the calculation of extinction coefficients using a Beer–Lambert–Bouguer equation. The second approach, which has been introduced in the original IFP1.4 paper[9], was based on a comparison of absorbance values for the protein at the main peak (692 nm or 694 nm) with the absorbance value at the 391 nm peak assuming the latter to have the extinction coefficient of the free BV which is 39,900 $M^{-1}cm^{-1}$. For determination of quantum yield, fluorescence signal of iRFP was compared to that of the equally absorbing IFP1.4 and Nile Blue dye (quantum yield is 0.27 in an acidic ethanol[30]).

pH titrations were performed using a series of buffers (100 mM NaOAc, 300 mM NaCl for pH 2.5–5.0, and 100 mM $NaH_2PO_4$, 300 mM NaCl for pH 4.5–9.0).

To study protein maturation, LMG194 bacterial cells were grown at 37°C overnight in a LB medium supplemented with ampicillin, kanamycin, and 2% of glucose. The next morning, the cells were centrifuged, resuspended, and cultured in RM medium with 0.002% arabinose, 0.001 mM IPTG, 100 μM ALA, and 50 μM $FeCl_3$ for 1 hour. Then, the cells were washed and cultured in RM medium supplemented with 0.001 mM IPTG, 100 μM ALA, and 50 μM $FeCl_3$ (no arabinose was added this time) at 37°C. Fluorescence intensity of the cell suspension was measured every hour initially and after longer time periods later.

Covalent BV attachment to the proteins was tested as it has been described[31].

## Mammalian plasmids and cell culture

A pShuttle-CMV vector (Stratagene) was utilized to construct plasmids for mammalian expression of both iRFP and IFP1.4 proteins. The FP genes were PCR-amplified and

inserted into the *Bgl*II and *Sal*I sites of the vector, thus generating pShuttle-CMV-iRFP and pShuttle-CMV-IFP1.4 plasmids.

HEK293 and HeLa cell lines were grown in Dulbecco's Modified Eagle Media (DMEM) containing 10% fetal bovine serum (FBS), penicillin-streptomycin, and 2 mM glutamine (Invitrogen). Cells were cultured in 35 mm glass bottom culture dishes with No. 1 cover glasses (MatTek Corporation). Plasmid transfections were performed using an Effectene reagent (Qiagen) according to the manufacturer's protocol.

For adenoviral infection, HeLa cells were grown in 60 mm Petri dishes until ~80% confluence and then infected with $3 \times 10^7$ PFU per dish.

## Characterization in mammalian cells

For FACS analysis of HeLa cells co-transfected with EGFP and NIR FPs, 488 nm Ar and 676 nm Kr laser lines and the respective 530/40 nm and 700LP nm emission filters were used. To quantify cells fluorescence, a mean fluorescent intensity of the double-positive population in the NIR channel was divided by a mean fluorescent intensity of the same population in the green channel, thus normalizing the NIR signal to the transfection efficiency.

Imaging of HeLa and HEK293 cells was performed 48 h after the transfection. Cells were imaged using an Olympus IX81 inverted epifluorescence microscope equipped with 200W metal halide arc lamp (Prior), a 100× 1.4 NA oil immersion objective lens (UPlanSApo, Olympus), and standard Cy5.5 filter set (665/45 nm exciter and 725/50 nm emitter) (Chroma).

Photobleaching measurements of cytoplasmically expressed NIR FPs in live HeLa cells were performed similarly to the purified proteins with the 100x objective substituted with a 60× 1.35 NA oil immersion objective lens (UPlanSApo, Olympus). Normalization of the curves was made the same way as for the purified proteins.

For protein degradation assay, HEK293 cells transfected with NIR FPs were treated with 1 mM of puromycin 48 hours post-transfection. To achieve brighter fluorescence signal, cells were kept with 25 μM of BV during the whole experimental course, starting 2 hours before the addition of the puromycin.

To study BV binding and BV influence on protein stability, HeLa cells were harvested 2 days post adenoviral infection and lysed by 3 freezing-thawing cycles. The lysates were clarified by centrifugation, and the total fluorescence was measured using the FluoroMax-3 spectrofluorometer (Jobin Yvon).

## Construction of adenoviral vectors

The adenovirus serotype V based particles containing the iRFP or IFP1.4 genes were created using an AdEasy XL Adenoviral Vector System (Stratagene) according to the manufacture's recommendations and then purified using a cesium chloride gradient centrifugation, as

described[32]. The viral titers were assessed by an Adeno-X Rapid Titer Kit (Clontech). Construction of adenoviruses encoding the GFP/S65T variant was described earlier[33].

## *In vivo* imaging

Albino C57BL/6 mice (female 6-8 weeks old, B6(Cg)-*Tyr*$^{c-2J}$/J, Jackson Laboratory) were intravenously injected with $2\times10^9$ infectious units of an adenovirus. Belly fur was removed using a depilatory cream, and the mice imaging was performed with an IVIS Spectrum instrument (Caliper LifeSciences) in epifluorescence mode equipped with 675/30 nm and 720/20 nm filters for excitation and emission, respectively, starting the second day after an infection. 250 nmol of BV were IV injected on the day 5 post-infection, and the mice imaging started 1 hour later. Quantitative measurements of fluorescence signal were made with a Living Image Software 4.0 (Caliper LifeSciences). For an *ex vivo* liver imaging, livers were dissected 1 hour after mice were injected with 250 nmol of BV. The isolated livers or spleens were imaged with the IVIS Spectrum instrument. All animal experiments were performed in an AAALAC approved facility using protocols approved by the Albert Einstein College of Medicine Animal Usage Committee.

## Protein imaging in phantom mouse

Bacterial plasmids encoding several far-red GFP-like FPs were kindly provided by Benjamin Glick (University of Chicago, USA) and Dmitry Chudakov and Konstantin Lukyanov (both from Institute of Bioorganic Chemistry, Russia). The recombinant GFP-like FPs were expressed in the LMG194 bacterial cells and then purified using the Ni-NTA agarose (Qiagen). The purified FPs were diluted to the equal concentrations of 16 μM, calculated based on the extinction coefficients at the chromophore absorbance maxima. The 5 μl volume of each FP was placed 15 mm deep inside into one of two available bores in a XFM-2 phantom mouse (Caliper LifeSciences). The bores were located at 7.0 mm and 18.1 mm distance from the imaging surface. Images were taken in 23 different combinations of the far-red and NIR excitation and emission channels using an epifluorescence mode of the IVIS Spectrum instrument. A signal-to-background ratio was calculated for each wavelength combination for each FP, using the phantom mouse without protein sample inside as a background reference. All quantitative measurements of fluorescence signal were performed utilizing the Living Image Software 4.0.

## References

1. Jobsis FF. Noninvasive, infrared monitoring of cerebral and myocardial oxygen sufficiency and circulatory parameters. Science. 1977; 198:1264–1267. [PubMed: 929199]

2. Hoffman RM. The multiple uses of fluorescent proteins to visualize cancer in vivo. Nat Rev Cancer. 2005; 5:796–806. [PubMed: 16195751]

3. Fischer AJ, Lagarias JC. Harnessing phytochrome's glowing potential. Proceedings of the National Academy of Sciences of the United States of America. 2004; 101:17334–17339. [PubMed: 15548612]

4. Sharrock RA. The phytochrome red/far-red photoreceptor superfamily. Genome biology. 2008; 9:230. [PubMed: 18771590]

5. Rockwell NC, Lagarias JC. A brief history of phytochromes. Chemphyschem. 2010; 11:1172–1180. [PubMed: 20155775]

6. Li L, Murphy JT, Lagarias JC. Continuous fluorescence assay of phytochrome assembly in vitro. Biochemistry. 1995; 34:7923–7930. [PubMed: 7794904]

7. Giraud E, et al. Bacteriophytochrome controls photosystem synthesis in anoxygenic bacteria. Nature. 2002; 417:202–205. [PubMed: 12000965]

8. Wagner JR, et al. Mutational analysis of Deinococcus radiodurans bacteriophytochrome reveals key amino acids necessary for the photochromicity and proton exchange cycle of phytochromes. The Journal of biological chemistry. 2008; 283:12212–12226. [PubMed: 18192276]

9. Shu X, et al. Mammalian expression of infrared fluorescent proteins engineered from a bacterial phytochrome. Science. 2009; 324:804–807. [PubMed: 19423828]

10. Giraud E, et al. A new type of bacteriophytochrome acts in tandem with a classical bacteriophytochrome to control the antennae synthesis in Rhodopseudomonas palustris. The Journal of biological chemistry. 2005; 280:32389–32397. [PubMed: 16009707]

11. Ulijasz AT, et al. Characterization of two thermostable cyanobacterial phytochromes reveals global movements in the chromophore-binding domain during photoconversion. The Journal of biological chemistry. 2008; 283:21251–21266. [PubMed: 18480055]

12. Campbell RE, et al. A monomeric red fluorescent protein. Proceedings of the National Academy of Sciences of the United States of America. 2002; 99:7877–7882. [PubMed: 12060735]

13. Stepanenko OV, et al. Understanding the role of Arg96 in structure and stability of green fluorescent protein. Proteins. 2008; 73:539–551. [PubMed: 18470931]

14. Sali D, Bycroft M, Fersht AR. Surface electrostatic interactions contribute little of stability of barnase. Journal of molecular biology. 1991; 220:779–788. [PubMed: 1870131]

15. Monera OD, Kay CM, Hodges RS. Protein denaturation with guanidine hydrochloride or urea provides a different estimate of stability depending on the contributions of electrostatic interactions. Protein Sci. 1994; 3:1984–1991. [PubMed: 7703845]

16. Muller L, et al. Evolutionary gain of function for the ER membrane protein Sec62 from yeast to humans. Molecular biology of the cell. 2010; 21:691–703. [PubMed: 20071467]

17. Scatchard G. The attraction of proteins for small molecules and ions. Ann. N.Y. Acad. Sci. 1948; 51:660–672.

18. Strack RL, et al. A noncytotoxic DsRed variant for whole-cell labeling. Nature methods. 2008; 5:955–957. [PubMed: 18953349]

19. Subramanian S, Srienc F. Quantitative analysis of transient gene expression in mammalian cells using the green fluorescent protein. J Biotechnol. 1996; 49:137–151. [PubMed: 8879169]

20. Warren L, et al. Highly efficient reprogramming to pluripotency and directed differentiation of human cells with synthetic modified mRNA. Cell Stem Cell. 2010; 7:618–630. [PubMed: 20888316]

21. Strack RL, et al. A rapidly maturing far-red derivative of DsRed-Express2 for whole-cell labeling. Biochemistry. 2009; 48:8279–8281. [PubMed: 19658435]

22. Lin MZ, et al. Autofluorescent proteins with excitation in the optical window for intravital imaging in mammals. Chemistry & biology. 2009; 16:1169–1179. [PubMed: 19942140]

23. Shcherbo D, et al. Near-infrared fluorescent proteins. Nature methods. 2010; 7:827–829. [PubMed: 20818379]

24. Shcherbo D, et al. Far-red fluorescent tags for protein imaging in living tissues. The Biochemical journal. 2009; 418:567–574. [PubMed: 19143658]

25. Morozova KS, et al. Far-red fluorescent protein excitable with red lasers for flow cytometry and superresolution STED nanoscopy. Biophysical journal. 2010; 99:L13–15. [PubMed: 20643047]

26. Kuo C, Coquoz O, Troy TL, Xu H, Rice BW. Three-dimensional reconstruction of in vivo bioluminescent sources based on multispectral imaging. Journal of biomedical optics. 2007; 12:024007. [PubMed: 17477722]

27. Xu H, Rice BW. In-vivo fluorescence imaging with a multivariate curve resolution spectral unmixing technique. Journal of biomedical optics. 2009; 14:064011. [PubMed: 20059249]

28. Gambetta GA, Lagarias JC. Genetic engineering of phytochrome biosynthesis in bacteria. Proceedings of the National Academy of Sciences of the United States of America. 2001; 98:10566–10571. [PubMed: 11553807]

29. Ho SN, Hunt HD, Horton RM, Pullen JK, Pease LR. Site-directed mutagenesis by overlap extension using the polymerase chain reaction. Gene. 1989; 77:51–59. [PubMed: 2744487]

30. Drexhage RS, a KH. Fluorescence quantum yield of oxazine and carbazine laser dyes. Journal of Luminescence. 1981; 24-25:709–712.

31. Lamparter T, et al. Biliverdin binds covalently to agrobacterium phytochrome Agp1 via its ring A vinyl side chain. The Journal of biological chemistry. 2003; 278:33786–33792. [PubMed: 12824166]

32. Luo J, et al. A protocol for rapid generation of recombinant adenoviruses using the AdEasy system. Nature protocols. 2007; 2:1236–1247. [PubMed: 17546019]

33. Cohen D, Brennwald PJ, Rodriguez-Boulan E, Musch A. Mammalian PAR-1 determines epithelial lumen polarity by organizing the microtubule cytoskeleton. The Journal of cell biology. 2004; 164:717–727. [PubMed: 14981097]
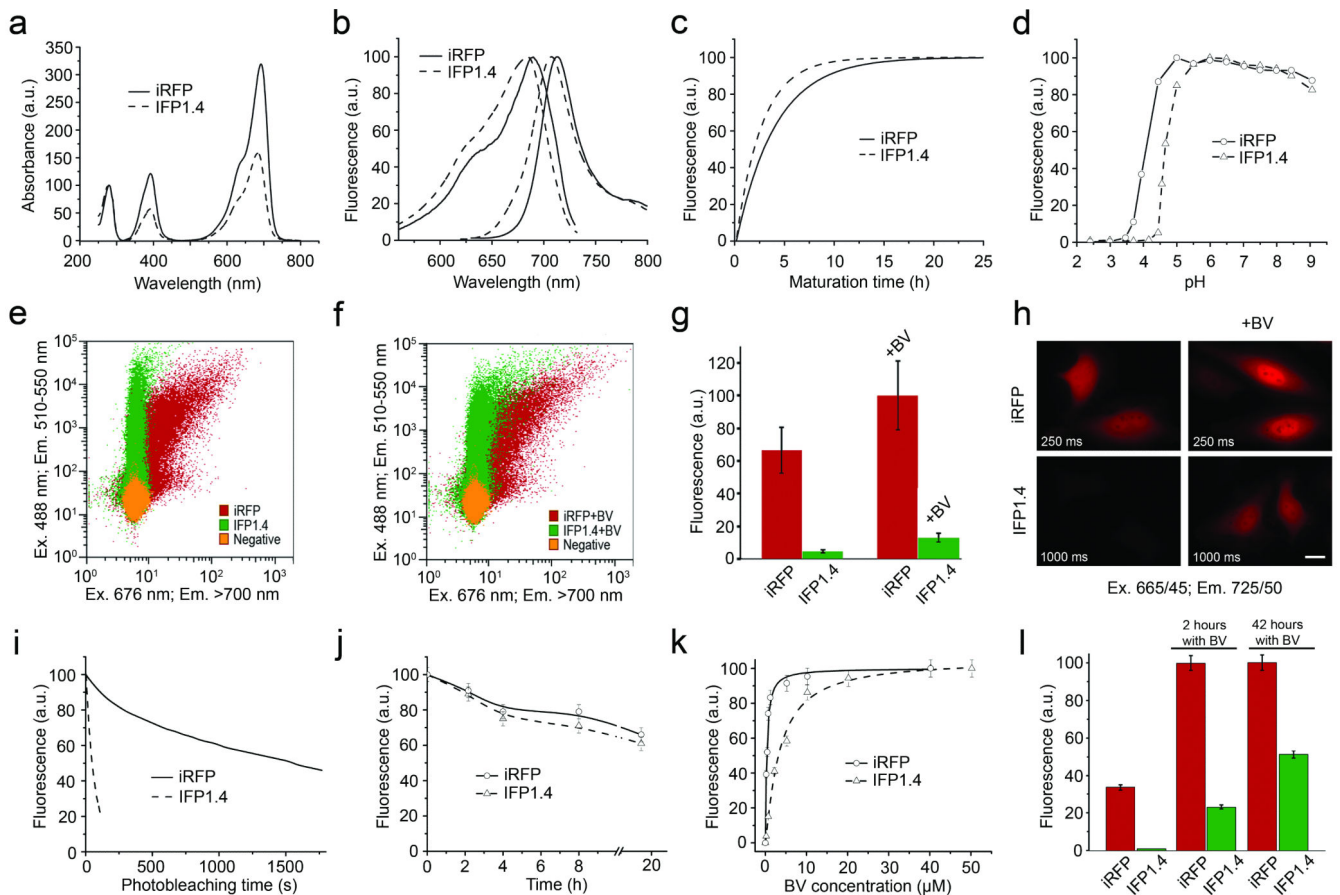
**Figure 1.** *In vitro* **properties of iRFP (solid lines and circles) and IFP1.4 (dashed lines and triangles)**

(**a**) Absorbance in arbitrary units (a.u.) with absorbance at 280 nm set to 100%. (**b**) Fluorescence excitation and emission spectra normalized to 100% for both proteins. (**c**) Fitted curves of the maturation kinetics in hours (h) in bacteria at 37°C. (**d**) Equilibrium pH dependence of fluorescence. (**e** and **f**) FACS dot-plots representing NIR fluorescence of iRFP and IFP1.4 (x axis) and green fluorescence from co-expressed EGFP (y axis) of transiently transfected HeLa cells not treated (**e**) or treated (**f**) with 25 μM of BV for 2 hours before analysis. A 676 nm laser line for excitation and a 700 nm long pass filter to collect emission from iRFP and IFP1.4 were used. (**g**) Mean NIR fluorescence intensity of the double-positive cells from (a) and (b) normalized to transfection efficiency (EGFP signal), absorbance of the respective protein at 676 nm, and overlap of the fluorescence spectrum of the respective protein with the transmission of the emission filter. (**h**) Fluorescent images of the transiently transfected HeLa cells with and without addition of 25 μM BV for 2 hours before imaging. Scale bar is 20 μm. (**i**) Photobleaching in HeLa cells. The curves were normalized to absorbance spectra and extinction coefficients of the proteins (calculated based on BV absorbance), spectrum of an arc lamp and transmission of a photobleaching filter. Plot represents the data obtained with endogenous BV but both proteins demonstrated no change in photostability after addition of exogenous BV. (**j**) Degradation of the proteins in HEK293 cells after treatment with 1 mM puromycin. Cells were incubated with 25 μM

BV to achieve a higher fluorescent signal. Protein concentration was assessed by measuring fluorescence intensity of crude cell lysates. (**k**) BV binding to iRFP and IFP1.4 proteins in HeLa cells. Cells were incubated with the respective amounts of BV during 2 hours before harvesting on the second day after adenovirus infection. Fluorescence intensity was measured in crude cell lysates and normalized to 100%. Lines are fitted based on the Scatchard equation. (**l**) Protein expression in HeLa cells 48 hours after adenovirus infection. Data for the cells without exogenous BV, with 25 μM of BV added 2 hours and 42 hours before the analysis are shown. Fluorescence intensities were normalized to the total cell number, excitation wavelength, emission collection bandwidth, and protein molecular brightness to represent the iRFP or IFP1.4 concentrations.
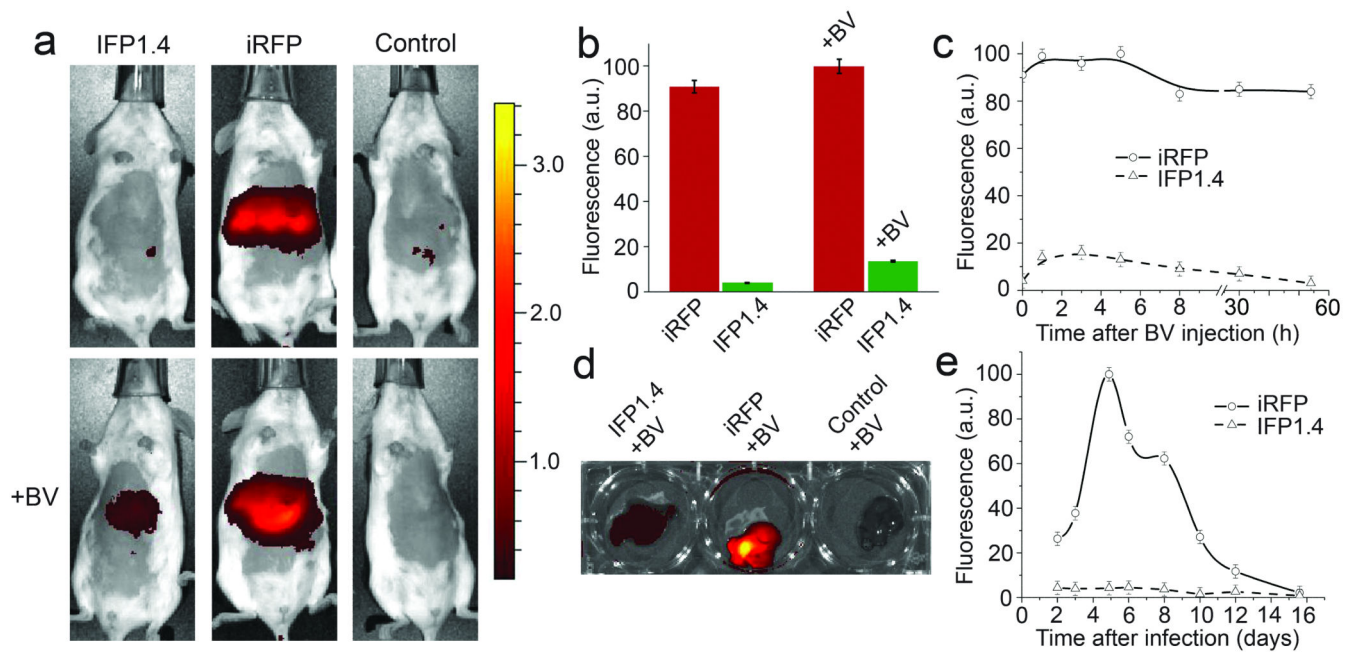
**Figure 2. Expression of iRFP in living mouse**
(**a**) Overlay of representative light and fluorescent images of iRFP or IFP1.4 adenovirus infected mice with and without injection of 250 nmol BV. A non-infected control mouse is shown on the right. The fluorescence images were acquired using IVIS Spectrum instrument equipped with 675/30 nm excitation and 720/20 nm emission filters. The color bar indicates the fluorescence radiant efficiency, multiplied by $10^9$. (**b**) Near infra-red fluorescence total radiant efficiency of the liver areas of the iRFP and IFP1.4 expressing mice in (a), normalized to the bandwidth of the excitation and emission filters. (**c**) Time course of the NIR fluorescence total radiant efficiency of the liver areas of the iRFP and IFP1.4 expressing mice in (a) after BV injection. (**d**) Overlay of the photograph and fluorescent image of the isolated livers from the BV-injected infected and non-infected (control) mice. (**e**) Time course of the NIR fluorescence total radiant efficiency of the liver areas of the mice not being injected with BV. The fluorescence signals were normalized to the bandwidth of the excitation and emission filters.
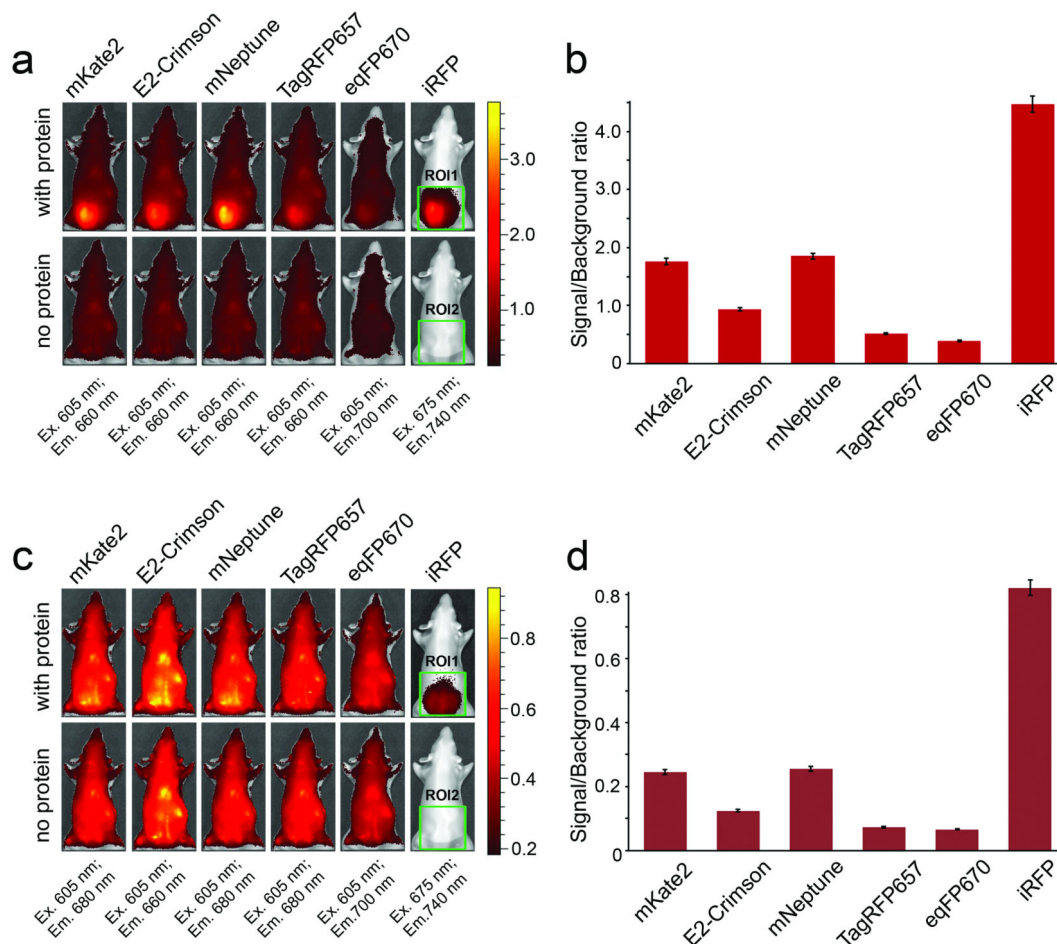
**Figure 3. Comparison of iRFP with far-red GFP-like proteins in mouse phantom**
Samples consisting of the equal amounts of the purified proteins of the same concentration
were placed inside of the phantom mouse in the bores located 7.0 mm (**a**) or 18.1 mm (**c**)
deep from the mouse surface. Each protein sample was imaged using epifluorescence mode
in several wavelength channels. A signal-to-background ratio in each channel was calculated
as (ROI1 - ROI2) / ROI2, where ROI1 or ROI2 were total radiant efficiencies of the
respective areas with and without the protein sample. Images for the highest signal-to-
background ratio for each protein are shown. The color bar indicates the fluorescence
radiant efficiency, multiplied by $10^8$. Panels (**b**) and (**d**) represent the highest signal-to-
background ratio values, calculated for the respective images in (a) and (c).

**Table 1**

*In vitro* properties of iRFP in comparison with IFP1.4.

| Protein | Absorbance maximum (nm) | Excitation maximum (nm) | Emission maximum (nm) | Extinction coefficient (M⁻¹cm⁻¹) (based on protein concentration) | Extinction coefficient (M⁻¹cm⁻¹) (based on extinction coefficient of BV) | Quantum yield (%) | Molecular brightness relative to IFP1.4 (%) | Photostability, $\tau_{50\%}$ (s) | pKa | Maturation at 37°C, 50% (h) | Conformational stability in GndCl, [D]50% (M) |
|---|---|---|---|---|---|---|---|---|---|---|---|
| **iRFP** | 692 | 690 | 713 | 85,000 | 105,000 | 5.9 | 120 | 450 | 4.0 | 2.8 | 2.9 |
| **IFP1.4** | 684 | 684 (684) | 707 (708) | 54,700 | 102,000 (92,000) | 7.7 (7.0) | 100 | 50 | 4.6 | 1.9 | 1.7 |

IFP1.4 characteristics from the original paper[9] are shown in parentheses. Spectroscopic parameters were determined in PBS at pH 7.5.